Investigating the Multiple Roles of Polyvinylpyrrolidone for A General Methodology of Oxide Encapsulation.

ARTICLE *in* JOURNAL OF THE AMERICAN CHEMICAL SOCIETY · MAY 2013

Impact Factor: 12.11 · DOI: 10.1021/ja4035335 · Source: PubMed

JACS
JOURNAL OF THE AMERICAN CHEMICAL SOCIETY
Article
pubs.acs.org/JACS

Investigating the Multiple Roles of Polyvinylpyrrolidone for a General Methodology of Oxide Encapsulation

Hang Sun,[†] Jiating He,[†] Jiangyan Wang,[‡] Shuang-Yuan Zhang,[∥] Cuicui Liu,[†] Thirumany Sritharan,[§,⊥] Subodh Mhaisalkar,[§,⊥] Ming-Yong Han,[∥] Dan Wang,*[,‡] and Hongyu Chen*[,†,⊥]

[†]Division of Chemistry and Biological Chemistry, Nanyang Technological University, 21 Nanyang Link, Singapore 637371, Singapore

[‡]State Key Laboratory of Multi-phase Complex Systems, Institute of Process Engineering, Chinese Academy of Sciences, Beijing 100190, People's Republic of China

[§]School of Materials Science and Engineering, Nanyang Technological University, 50 Nanyang Avenue, Singapore, 639798

[∥]Institute of Materials Research and Engineering, Agency for Science, Technology and Research, 3 Research Link, Singapore 117602, Singapore

[⊥]Singapore-Berkeley Research Initiative for Sustainable Energy, 1 Create Way, Singapore 138602, Singapore

Supporting Information

ABSTRACT: Growing oxide shells on seed nanoparticles requires the control of several processes: (a) the nucleation and growth of the shell material; (b) the "wetting" of the shell material on the seeds; and (c) the aggregation of the nanoparticles. These processes are influenced by a number of factors, many of which are related. Without understanding the interdependence of these contributing factors, it is difficult to circumvent problems and achieve rational synthesis. We first did a case study on encapsulating Au nanoparticles with ZnO to understand the multiple roles of polyvinylpyrrolidone (PVP) and their dependence on other factors. We developed a general method for coating ZnO on a variety of seeds, including metals, oxides, polymer nanoparticles, graphene oxide, and carbon nanotube. This method can be further extended to include Fe_3O_4, MnO, Co_2O_3, TiO_2, Eu_2O_3, Tb_2O_3, Gd_2O_3, β-$Ni(OH)_2$, ZnS, and CdS as the shell materials. The understanding obtained in this systematic study will aid rational design and synthesis of other core−shell nanostructures.

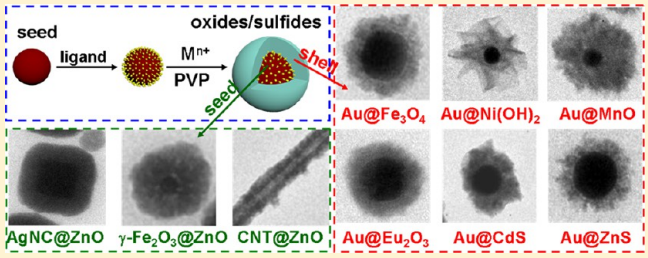

INTRODUCTION

Combining metal and semiconductor components in precisely controlled nanostructures has recently become a hot research topic. The coupling of the plasmonic effects of metal nanoparticles (NPs) with semiconductor properties has shown great promise in applications such as photocatalysis,[1] optoelectronics,[2] and laser.[3]

Core−shell nanostructure is the simplest motif in two-component systems, but there are still significant challenges in the synthetic control.[4] For two materials of the same type, the synthesis of core−shell nanostructure is typically straightforward, for example, Au@Ag,[5] CdSe@CdS,[6] SiO_2@TiO_2,[7] Fe_2O_3@TiO_2,[7] etc. However, for two dissimilar materials, the shell synthesis remains a challenge because additional controlling factors are required. In coating oxides on metal cores, for example, sometimes the cores are incompletely covered; sometimes there are multiple oxide domains on each core; sometimes the particles aggregate together forming large clusters; and sometimes the product contains a mixture of the above structures (Figure 1). Thus, it is often difficult to interpret the underlying causes and tune their combined effects. In this work, we aim to isolate the controlling factors and study them individually, so that the knowledge gained can be used to

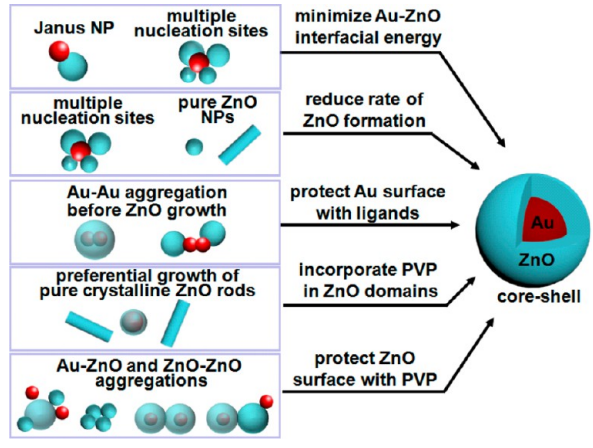

Figure 1. Schematics illustrating the measures for targeting the typical problems in the synthesis of core−shell nanostructures.

Received: April 9, 2013
Published: May 24, 2013

   dx.doi.org/10.1021/ja4035335 | J. Am. Chem. Soc. 2013, 135, 9099−9110

develop a synthetic approach that is rational, general, reproducible, and gives specific structural control.

Typically, there is a large interfacial energy between an oxide and a metal, mainly because of their lattice mismatch and lack of chemical interaction. Thus, when growing an oxide on the surface of metal NPs, it often forms granular domains to minimize the unfavorable oxide−metal interface. From the point of view of interfacial energy, such a granular growth mode is favorable, whereas the formation of a spread-out shell is unfavorable. Unless there is a way to mediate the oxide−metal interface, the lattice matching or chemical interactions can hardly be tuned.[8] In particular, for hybrid NPs synthesized under high-temperature using nonpolar solvents,[9] there is barely any ligand/surfactant between the crystalline phases of oxide and metal, making their interface untunable. If two materials are intrinsically unmatched, there is few means to force them into an unfavorable core−shell configuration.[10]

An obvious alternative is to embed ligand/surfactant molecules between the two materials to allow interface tuning. Yet this ligand must also stabilize the NPs in the synthetic solutions. Syntheses of many oxides, except for silica, require the use of metal salts as precursors, which could cause aggregation of the seed NPs. Therefore, finding a compatible ligand/surfactant is challenging, and this could be the reason shells of metal oxides have rarely been synthesized, even though their corresponding pure oxide NPs are common. So far, the method development for oxide encapsulation is rather case-specific.

Coating silica on metal NPs is relatively well-known, and several ligands and surfactants have been reported. Typically, the reaction is carried out in polar solvents, and the seed surface is functionalized with −Si−OH or −COOH groups to render it amenable for silica adsorption.[11] Yet this method has not been extensively applied to other oxide coatings, presumably because of aggregation problems. Wang et al. extended this approach to develop a general method for coating sulfides: Using thiobenzoate as the ligand, the surface of Au NPs was modified such that a thin layer of CuS or Ag_2S can be coated.[12] Both the ligand and the intermediate wetting layer were critical in facilitating the subsequent deposition of the sulfides (ZnS, CdS, NiS, CuS, or Ag_2S) on the NPs.

On the other hand, polyvinylpyrrolidone (PVP) has been used to help deposit oxides on NPs, forming flower-like[13] and core−shell hybrid NPs.[14] As discussed in the following, the amphiphilic PVP plays multiple roles such as tuning the NP−oxide interfacial energy, stabilizing the ZnO NPs against aggregation, interfering with oxide crystal formation, etc. It is difficult to find a single additive to replace all of these roles. Thus, when PVP is replaced or tuned in concentration, many aspects of the product NPs change, making it difficult to distinguish the individual roles. To date, the synthetic scope of oxide−metal hybrid NPs is still very limited, and developing a general synthetic approach remains a challenge.

Here, we present a systematic study of the multiple roles of PVP in the synthesis of metal−oxide hybrid NPs. Different additives are used to probe and replace the individual roles of PVP, and careful control experiments were carried out to compare their effects. The roles of PVP are analyzed among other factors, in the context of tuning interfacial energies and controlling nucleation and growth. With the new understandings, a general method is developed for coating oxides and sulfides: NPs, nanowires (NWs), and nanotubes of different compositions, different surface ligands, and different oxides and sulfides were combined to create a large variety of core−shell nanostructures.

RESULTS AND DISCUSSION

We used Au@ZnO NPs as a model system for understanding the multiple controlling factors. The synthesis of such core−shell nanostructures has not been reported, although eccentric or Janus (two-faced) Au−ZnO NPs were known.[15] It is a typical system where neither a ligand nor a surfactant alone can solve the encapsulation problem. Indeed, the ZnO system is particularly problematic because of the anisotropic nature of wurtzite ZnO crystals.[16] We found that 4-mercaptobenzoic acid (ligand **1**) can reduce the Au−ZnO interfacial energy, just like in the Au−silica system.[11c,17] Combined with the help of surfactant PVP, Au@ZnO NPs can be easily synthesized. It was found that the two additives also played several other important roles, which will be analyzed below.

1. Synthesis of Au@ZnO Core−Shell NPs. As-synthesized, citrate-stabilized AuNPs (40 nm) were treated with ligand **1** (final concentration of 15 μM, same below) at 60 °C for 2 h. The functionalized Au NPs were isolated by centrifugation and dispersed in an aqueous PVP solution (M_w = 40 000 g mol^{-1}, 110 mM in terms of monomer concentration, same below). Hexamethylenetetramine (HMTA, 1 mM) was then added, followed by $Zn(NO_3)_2$ (1 mM) to cause ZnO formation.[18] The reaction was incubated at 95 °C for 3 h, and the resulting Au@ZnO core−shell NPs were isolated by centrifugation.

Here, the **1**-modified AuNPs were used as the seeds for the surface nucleation of ZnO via the in situ hydrolysis and condensation of Zn^{2+} ions. $Zn(NO_3)_2$ could be replaced by other zinc salts such as $Zn(CH_3COO)_2$.[19] HMTA can hydrolyze in water to give NH_3.[20] Thus, the basicity of the solution was slowly changing, which ensured controlled hydrolysis. Other bases such as Na_2CO_3 could also replace HMTA in giving ZnO, but their synthetic control was more challenging because of the faster reaction rates (see section 8).

Figure 2a shows the transmission electron microscopy (TEM) image of the Au@ZnO core−shell NPs, where the

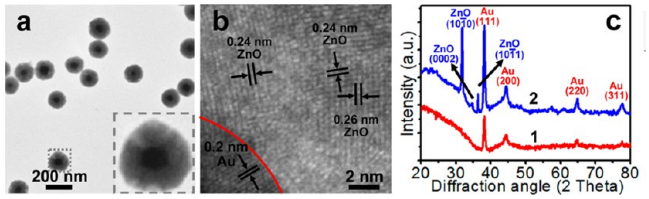

Figure 2. (a) TEM image of Au@ZnO core−shell NPs (d_{Au} = 40 nm); a magnified NP is shown in the inset. (b) HRTEM image showing the polycrystalline nature of the ZnO domain. (c) XRD patterns of (1) Au and (2) Au@ZnO NPs.

Au cores show a darker contrast than the ZnO shells. The NPs were uniform in size with an average diameter of 120 nm. The ZnO shells were spherical with smooth outline, without any granular or crystalline appearance. This is quite unusual for ZnO nanocrystals.[1c,15] In a typical high-resolution TEM (HRTEM) image (Figure 2b), the ZnO domains appeared polycrystalline with a large number of small and randomly oriented crystallites. The lattice spacing was measured as 0.24 and 0.26 nm, consistent with the $(10\bar{1}1)$ and (0002) planes of wurtzite ZnO structure, respectively.[21] As shown in Figure 2c, the X-ray diffraction (XRD) pattern agreed with the $(10\bar{1}0)$,

dx.doi.org/10.1021/ja4035335 | J. Am. Chem. Soc. 2013, 135, 9099−9110

(0002), (10$\bar{1}$1) planes of wurtzite ZnO structure,[18b] and not with the typical $Zn(OH)_2$ peaks.[22] The remaining peaks could be indexed to the face-centered-cubic Au (111), (200), (220), and (311) planes.[23]

2. General Analysis of the Controlling Factors. The typical precursors for synthesizing metal oxides are the soluble forms of metal salts, which could cause the aggregation of seed NPs. Because the use of metal salts is unavoidable, the best strategy is to apply suitable ligand/surfactant to help stabilize the NPs.

Two additives were used in our system: ligand **1** was used to modify the Au surface, whereas the surfactant PVP was used to bind the Au and ZnO surfaces. Both of them are of importance. Figure 3a shows a control experiment without using PVP. Only

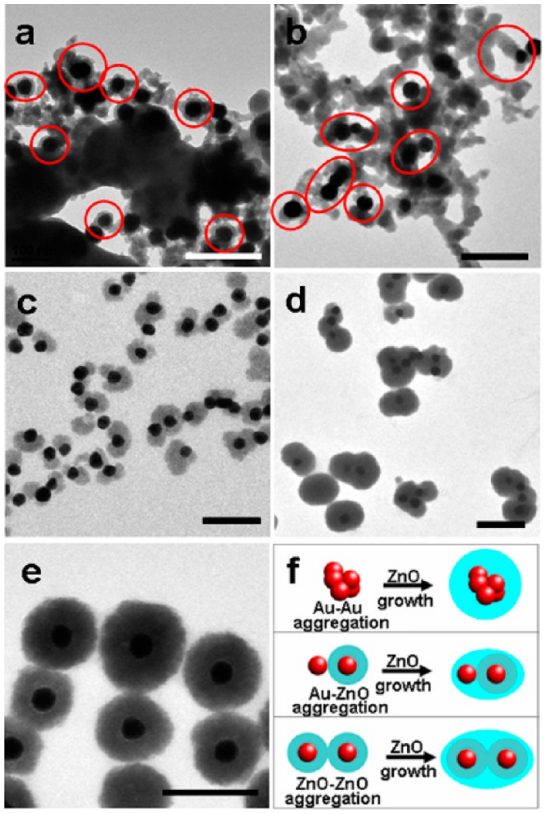

Figure 3. Investigating interfaces and aggregation. (a,b) TEM images of Au–ZnO hybrids prepared in the absence of PVP, from Au seeds (d_{Au} = 40 nm) that were modified with either (a) ligand **1** or (b) **4**; (c,d) Au–ZnO hybrids prepared without ligand but in the presence of PVP, where the seeds were incubated with PVP for (c) 0, or (d) 2 h; (e) Au@ZnO hybrids prepared in the presence of PVP, from Au seeds that were modified with ligand **4**. (f) Schematics illustrating the difference between Au–Au, Au–ZnO, and ZnO–ZnO aggregation, before and after ZnO encapsulation. Scale bar: 200 nm.

a thin layer of ZnO formed on the AuNPs, but there was extensive growth and aggregation of pure ZnO NPs. On the other hand, in the control experiment without using **1**, only partial ZnO shells were formed on the Au seeds (Figure 3c). Hence, neither of the compounds individually was able to solve both problems of aggregation and shell formation.

Ligand **1** was chosen to reduce the Au–ZnO interfacial energy,[11c] but this role was complicated by the necessary addition of amphiphilic PVP. Moreover, because PVP interacts strongly with Zn^{2+} ions, it can interfere with ZnO crystal formation, thus affecting the nucleation and growth of ZnO domains. To resolve these entangled factors, we have to separate their individual roles by using substitutes.

3. Effects of Surface Ligand. To identify the effects of Au ligands, we need to first prove that the ligands did bind to the Au surface. In surface-enhanced Raman scattering (SERS), it is known that the Raman signal of molecules can be greatly enhanced when they are in the close vicinity of a metal surface.[24] In the above synthesis, **1** was SERS-active, and the resulting Au@ZnO NPs did exhibit strong SERS signal that was characteristic of **1** (Figure 4a).[25] This indicates that the ligand remained on the Au surface even after the ZnO encapsulation.[8]

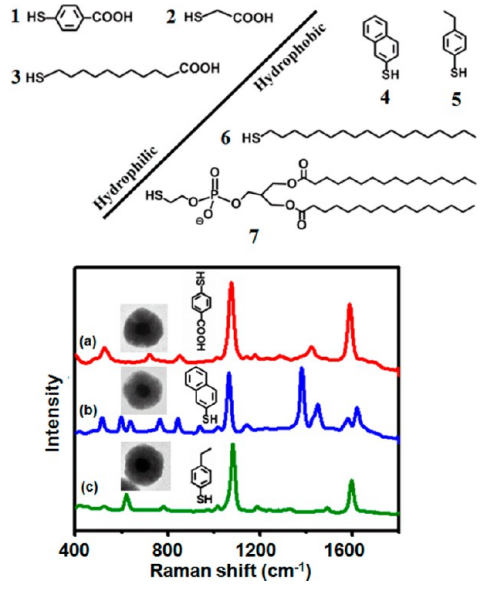

Figure 4. Ligand generality. Chemical structures of the hydrophilic and hydrophobic ligands that have been successfully used for creating Au@ZnO core–shell NPs. (a–c) SERS spectra of the core–shell Au@ZnO NPs that were prepared by using either (a) 4-mercaptobenzoic acid, (b) 2-naphthalenethiol, or (c) 4-ethylthiolphenol as the ligand.

Ligand **1** has a –SH group that can anchor on the Au surface, and a –COOH group that can interact with ZnO surface (Au–**1**–ZnO, Figure 5b). While Au does not interact strongly with ZnO, the mediating molecule **1** can interact with both, reducing the Au–ZnO interfacial energy.

When 2-naphthalenethiol (**4**) was used as the ligand in place of **1**, similar core–shell structured Au@ZnO NPs were obtained (Figure 3e). This was surprising because the nonpolar **4** is known to interact poorly with polar silica. Hence, interaction with ZnO was also expected to be poor. The ligand scope was further expanded (Figure 4) to include two more thiol ligands with –COOH end groups, 2-mercaptoacetic acid (**2**) and 11-mercaptoundeconoic acid (**3**), and three more hydrophobic thiol-based ligands, 4-ethylthiophenol (**5**), 1-octadecanethiol (**6**), and 1,2-dipalmitoyl-*sn*-glycero-3-phosphothioethanol (sodium salt) (**7**, a thiol-ended phospholipid). Core–shell Au@ZnO NPs were obtained in all cases,[19] highlighting the generality in the use of surface ligands. Yet this also showed that the unexpected success in using hydrophobic ligand was not an isolated case. Among the ligands used, **1**, **4**, and **5** were SERS active. Their signals can be clearly identified after ZnO encapsulation (Figure 4),[19,26] confirming their presence at the Au surface.

dx.doi.org/10.1021/ja4035335 | J. Am. Chem. Soc. 2013, 135, 9099–9110

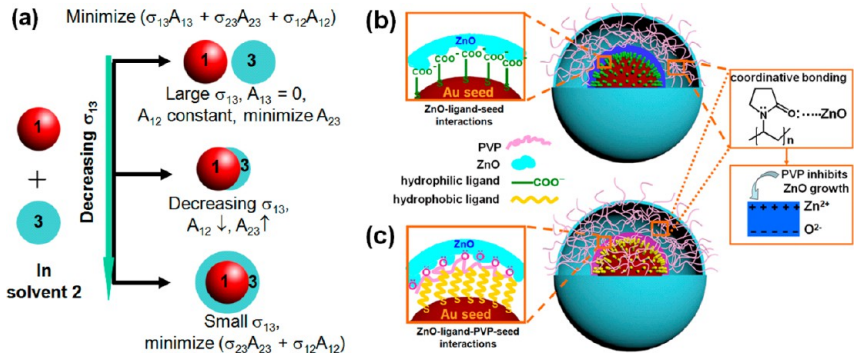

Figure 5. Controlling the "wetting" of ZnO on Au seeds. (a) Equilibrium configurations for two immiscible liquid droplets 1 and 3 in solvent 2; and schematics illustrating (b) the Au–ligand–ZnO and (c) the Au–ligand–PVP–ZnO interactions in Au@ZnO NPs.

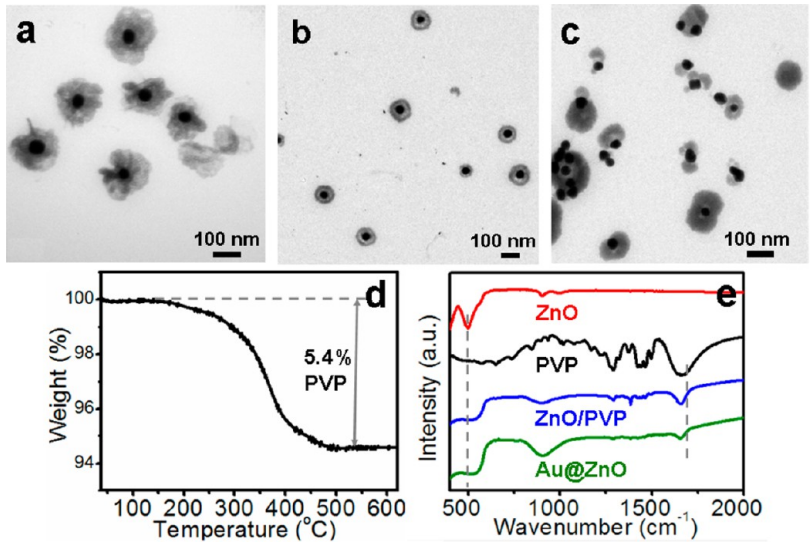

Figure 6. PVP incorporation in ZnO. Using high molecular weight PVP (360 000), the segregated PVP domains in the Au@ZnO NPs (d_{Au} = 40 nm) can be directly observed in the TEM images: (a) ligand **1**, (b) ligand **4**, and (c) no ligand was used. (d) TGA analysis of the Au@ZnO core–shell NPs that were derived from low molecular weight PVP (40 000). (e) IR spectra of pure ZnO rods, pure PVP, PVP doped ZnO NPs, and PVP-doped Au@ZnO core–shell NPs (from top to bottom), respectively.

To investigate the ligand–ZnO interaction without interference from the surfactant PVP, we tried to grow ZnO directly on the ligand-modified Au seeds. In the absence of PVP, ZnO could form a continuous shell on the Au seeds modified by **1** (Figure 3a) or **2**, but not on those modified by **4** (Figure 3b) or **7**.[19] Despite the serious aggregation of ZnO NPs in these samples, the "wetting" property of ZnO on the seeds can be clearly discerned (it was not a real wetting because both phases were solid; see section 4). As expected, ZnO did not interact well with the hydrophobic ligands on the Au surface. Hence, the surfactant PVP must have played an important role in the full ZnO encapsulation of **4**-modified seeds in Figure 3e.

PVP is an amphiphilic polymer, with polar amine and carbonyl groups on one side and nonpolar methylene groups on the other. Thus, the nonpolar side can interact with the hydrophobic ligands, whereas the polar side can interact with ZnO (Au–**4**–PVP–ZnO, Figure 5c). In a set of control experiments, we replaced PVP with hydrophilic polyethyleneglycol (PEG), which can interact with ZnO (see Section 6) but not with hydrophobic ligands. As expected, PEG had essentially no effect in improving the "wetting" of ZnO domains: Continuous shells formed on the hydrophilic Au seeds, but not on the hydrophobic ones,[19] just like the results shown in Figure 3a,b. Hence, the amphiphilicity of PVP was essential in the ZnO encapsulation when hydrophobic ligands were used.

These results show that the Au–**1**–ZnO and Au–**4**–PVP–ZnO interactions are fundamentally different (Figure 5b,c). Yet they both can greatly improve the ZnO encapsulation. The Au–ZnO interfacial energies cannot be easily measured at the nanoscale, because it is difficult to control the extent of ligand coverage and the exact strength of molecular interactions. Yet the trend of improving the interfacial interactions can be clearly correlated to the changes in Au–ZnO morphology, and this correlation can be analyzed using the theory below.

4. Effects of Interfacial Energy. For two immiscible liquid droplets suspended in a third immiscible liquid solution (Figure 5a), there are three interfacial energies: σ_{12}, σ_{13}, and σ_{23}. Whether one droplet can engulf the other depends on the relative strength of these interfacial energies.[8,27] Basically, the system tends to minimize the total surface energy ($\sigma_{12}A_{12} + \sigma_{23}A_{23} + \sigma_{13}A_{13}$). For example, if 1 "hates" (i.e., has poor interactions with) solvent 2, but 3 "likes" both 1 and 2, then droplet 3 can engulf droplet 1, forming an intermediate layer between 1 and 2; if 3 "hates" 1, then engulfing cannot occur.

In this analysis, when σ_{12} and σ_{23} are constants, reducing σ_{13} will cause A_{13} to increase. Our experimental observations were

dx.doi.org/10.1021/ja4035335 | J. Am. Chem. Soc. 2013, 135, 9099–9110

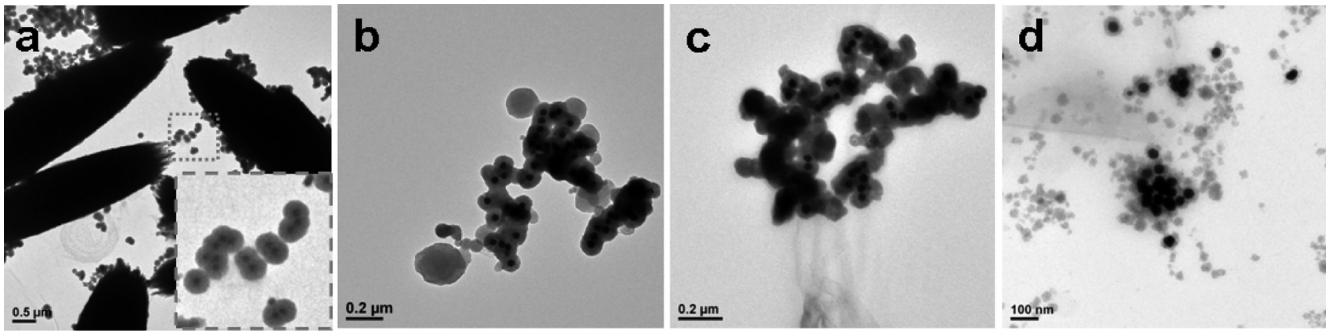

Figure 7. Interfering with the growth of ZnO nanocrystals. TEM images of Au/ZnO nanohybrids (d_{Au} = 40 nm) prepared by using **1** as the ligand in the presence of the following surfactant: (a) 50 mM PVP, (b) 110 mM VP monomer, (c) 110 mM PEG, M_w = 35 000 g mol^{-1}, and (d) 110 mM PSS, M_w = 90 000 g mol^{-1}.

consistent with this interpretation; that is, improving the Au−ZnO interaction improved the "wetting" of ZnO on the Au seeds. If the ZnO domain interacts poorly with the Au surface (large σ_{13}), the system will minimize the Au−ZnO interface (A_{13} = 0, i.e., no adsorption) and maximize the interactions within the ZnO domain. The tendency then is to form nearly spherical ZnO domains to minimize the surface to volume ratio (S/V, minimal surface also means maximal internal interactions). With improving Au−ZnO interaction, the ZnO "wets" the Au surface better, progressively expanding the Au−ZnO interface at the cost of the Au−solvent interface.

These thermodynamic analyses are more accurate if phase 3 is a liquid and equilibrium configuration can be readily achieved. However, in our system, both Au and ZnO were solids. They cannot flow into the preferred configuration if they did not form at near equilibrium conditions. Near equilibrium may be attained during slow growth, where the ZnO self-assembly should take low-energy pathways. This was probably the case for Figure 3b,c, where the surface nucleation of ZnO was not rapid enough to achieve full encapsulation. When the Au−ZnO interface was not improved, we found that it was extremely difficult to force Au−ZnO into complete core−shell structure (thermodynamically unfavorable). Yet it is possible that fast ZnO deposition (with additional chemical driving force) may lead to multiple nucleation sites on a seed.

Thus, the final Au−ZnO configuration should depend on both thermodynamic and kinetic factors. The latter includes the nucleation of ZnO on the seeds and its subsequent growth, both of which depend on the rate of ZnO formation (section 8).

5. Incorporation of PVP in Au@ZnO. The presence of PVP in ZnO domain was difficult to identify when low molecular weight PVP was used (40 000): The ZnO domain in Figure 2a was not uniform in contrast, and in Figure 3e, a thin, low-contrast layer was just visible between Au and ZnO. Composed of H, C, N, and O, PVP shows a lighter contrast in TEM images than ZnO. Yet this effect is not obvious unless the PVP domain is sufficiently large. When we increased its molecular weight to 360 000 g mol^{-1}, the segregated PVP domains became clearly observable. Using **1** as the ligand, the resulting ZnO domains appeared hollow with uneven contrast, but there is no obvious gap between Au and ZnO (Figure 6a). In contrast, when **4** was used as the ligand, there was a clear gap between Au and ZnO (Figure 6b; see more examples in the Supporting Information), supporting the direct adsorption of PVP on the **4**-modified Au surface. In the absence of both ligands, PVP was found to directly adsorb on the Au surface, often in isolated domains (Figure 6c). In consequence, the ZnO coating was often incomplete.

In the above three cases, the distinct locations of the sizable PVP domains were readily reproducible in repeated experiments and among a large number of particles.[19] Similar to ZnO domains, the "wetting" characteristics of the PVP domains on the Au seeds can also be analyzed on the basis of the interfacial energies. The PVP−solvent interfacial energy did not change, but the Au−PVP and Au−solvent interfaces depended on the ligands. With polar ligands, PVP cannot directly adsorb on the **1**-modified Au surface (large interfacial energy due to lack of interactions); with nonpolar ligands, PVP could fully cover the **4**-modified Au surface (small interfacial energy due to van der Waals and hydrophobic interactions). Although PVP can directly interact with Au,[14b] the interaction was clearly intermediate between the weak Au−**1**−PVP and strong Au−**4**−PVP interactions. As a result, the PVP domains formed islands instead of complete shells (Figure 5a). Our observations in Figure 6a−c were in general consistent with these analyses.

In the above cases, a significant amount of PVP (as low-contrast domains) was clearly incorporated inside the ZnO shells,[18b] as opposed to surface adsorption. For PVP of low molecular weight (M_w = 40 000 g mol^{-1}), TEM observation was not conclusive (Figure 2a). Hence, thermogravimetric analysis (TGA) was carried out; there was about 5.4% of weight loss over the temperature range of 150−500 °C (Figure 6d). Considering the densities of ZnO and PVP (5.6 and 1.2 g cm^{-3}, respectively), the PVP domains should occupy an equivalent of 21% of the total volume. Because the sample had been thoroughly washed before drying, only a small percentage of this 21 vol % PVP could exist on the ZnO surface (Figure 5b,c). Thus, the TGA data lent further support to the incorporation of PVP inside the ZnO domains. In the Fourier transform infrared (FTIR) spectrum of Au@ZnO NPs, the observation of C═O stretching at 1655 cm^{-1} (Figure 6e) was consistent with PVP incorporation.[28] This peak was red-shifted from the 1633 cm^{-1} of free PVP, indicating weak coordinative bonding of C═O to Zn^{2+} at the ZnO/PVP interface.[18b] The peak at 525 cm^{-1} can be assigned Zn−O vibration. In comparison to the spectrum of pure ZnO rods, this peak was blue-shifted from 498 cm^{-1} with significant broadening. These observations are consistent with small ZnO crystalline particles.[29]

6. Effect of PVP on ZnO Crystals. The incorporation of PVP in ZnO domains has a major impact on the size and morphology of the ZnO nanocrystals. In the absence of PVP, wurtzite ZnO prefers to grow anisotropically along the [0001]

dx.doi.org/10.1021/ja4035335 | J. Am. Chem. Soc. 2013, 135, 9099−9110

direction because of its hexagonal structure. Direct growth of ZnO in solution often gives large rod-like structures.[19]

However, in the presence of PVP (eq 110 mM of monomer), spherical ZnO particles formed instead of rod-like products. These spherical ZnO domains appeared polycrystalline (Figures 2a, 6a–c). Here, the $[PVP_{monomer}]/[Zn^{2+}]$ ratio was extremely high at about 110, which is similar to that in the literature reports.[14c] When this ratio was decreased to 50, some large rod-like ZnO mesocrystals[30] were observed along with spherical Au@ZnO NPs (Figure 7a). Obviously, a few ZnO crystals were able to grow extensively while most of the Au@ZnO NPs did not. Because both products were obtained in the same solution, homogeneous properties such as the viscosity of the solution or the reaction rates of Zn^{2+} cannot explain the results. A feasible explanation is that there are two parallel growth modes: a fast growth without PVP doping and a slow one with doping. Hence, in our method, the high PVP concentration was probably necessary to suppress the preferential growth of the nondoped ZnO crystals.

In addition to PVP, many other molecules were found to interfere with ZnO crystal formation: *N*-vinyl-2-pyrrolidone (VP, i.e., the monomer of PVP, 110 mM, Figure 7b), poly(ethylene glycol) (PEG,[30,31] M_w = 35 000 g mol^{-1}, 110 mM, Figure 7c), poly(sodium 4-styrenesulfonate) (PSS, M_w = 90 000 g mol^{-1}, 110 mM, Figure 7d), and even tiny amounts of ligand **1** or **4** (estimated residue concentration on the order of 10^{-7} M, Figure 3a,b). In their presence, the formation of ZnO rods was suppressed, and the resulting ZnO NPs had rounded outline and appeared polycrystalline. While the thiol-based ligands were extremely effective in interfering with ZnO growth, they tended to cause serious aggregation.

7. Controlling NP Aggregation. In our system, the aggregation of NPs came in several different forms: Au–Au, Au–ZnO, and ZnO–ZnO aggregation (Figure 3f). Without analyzing their different causes, it will be difficult to find a common solution. In general, salts such as $Zn(NO_3)_2$ can shield the charge repulsion among NPs and promote their aggregation; covering NPs with ligands or surfactants can reduce aggregation because they introduce additional charge and/or steric repulsion. PVP is a long polymer with multiple binding sites, which can interact with both Au[14b] and ZnO.[18b] Because each AuNP can be tethered with multiple PVP molecules and each PVP can bind to multiple Au or ZnO NPs, PVP can actually promote aggregation to a certain extent, particularly during a long incubation period.

When only PVP was used in the reaction without ligands, $Zn(NO_3)_2$ caused rapid aggregation of the citrate-stabilized AuNPs. This should only occur at the initial stage, because once ZnO shells were formed, PVP was quite effective in preventing the ZnO–ZnO aggregation. Pretreating the citrate-stabilized AuNPs with PVP (2 h) should be able to reduce the salt-induced aggregation, but the incubation with PVP in itself can also cause Au–Au aggregation (Figure 3d). When only **1** was used without PVP, the **1**-modified AuNPs were relatively stable in the presence of $Zn(NO_3)_2$, but the ZnO–ZnO aggregation was very severe (Figure 3a).

In contrast, when both PVP and **1** were used, one can prevent PVP from simultaneously interacting with Au and ZnO: Ligand **1** is a stronger ligand than PVP. It preferentially adsorbed on the Au seeds, fully covering them and reducing both the salt-induced and the PVP-induced Au–Au aggregation. Once ZnO shells were formed, PVP can reduce the ZnO–ZnO aggregations. On the other hand, when PVP on itself cannot fully cover the unmodified Au seeds (Figure 6c), the exposed Au surface is prone to Au–ZnO aggregation. When hydrophobic ligands such as **4** were used, PVP fully covered the **4**-modified AuNPs, reducing all aggregations (Figure 6b).

In Figure 7b,c, it can be observed that VP or PEG is not effective in reducing ZnO–ZnO aggregation. While PSS can prevent ZnO–ZnO aggregation, it seemed to have greatly promoted Au–Au aggregation (Figure 7d).

8. Nucleation and Growth of ZnO. In this system, the growth of ZnO could take several pathways: (a) it can nucleate on its own forming pure ZnO NPs (homogeneous nucleation), (b) it can deposit on the surface of the ligand-modified Au seeds (heterogeneous nucleation on Au), or (c) it can deposit on the surface of existing ZnO domains (heterogeneous nucleation on ZnO). These three competing processes have different "activation barriers", which essentially depend on the surface energy of the newly added ZnO domain: In homogeneous nucleation, the initially formed ZnO domains will be very small with a large S/V ratio. Moreover, they have poor interactions with the solvent (large σ_{23}, Figures 5a and 8).

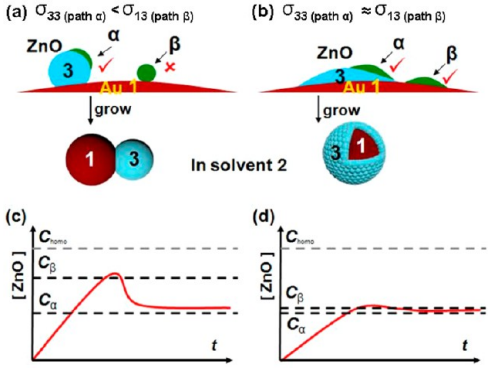

Figure 8. (a,b) Schematics illustrating the choice of competitive nucleation pathways when the Au–ZnO interfacial energy is (a) high or (b) low. (c,d) Plots of ZnO solubility versus time, highlighting the different growth behavior when the Au–ZnO interfacial energy is (c) high or (d) low.

Thus, the homogeneous nucleation barrier is the highest among the three. In the heterogeneous nucleation on ZnO, the new ZnO domain strongly interacts with the ZnO seeds. Indeed, the interaction should be as strong as the internal interactions within the ZnO domains (i.e., $\sigma_{33} = 0$). Thus, the newly added ZnO domain should completely "wet" the ZnO seed (path α in Figure 8a), leading to the lowest activation barrier.

As discussed in section 4, usually $\sigma_{13} < \sigma_{23}$ (Figure 5a); otherwise, it will be energetically unfavorable for ZnO to nucleate on the Au surface, and homogeneous nucleation will occur instead. If the newly formed ZnO domain cannot completely "wet" the Au surface (path β in Figure 8a), forming a Au–ZnO interface ($\sigma_{13}A_{13}$) is still more favorable than forming an equivalent sized ZnO–solvent interface ($\sigma_{23}A_{23}$). Thus, this nucleation barrier is lower than that for homogeneous nucleation, but higher than that for heterogeneous nucleation on ZnO (Figure 8c).

The ZnO deposition is driven by its oversaturation in the system, which is a function of the net rate of ZnO formation, that is, after subtraction of the rate of ZnO depletion (nucleation and growth). In the absence of any seeds, the solubilized form of ZnO has to build up to a critical concentration (C_{homo}), before the burst of homogeneous

dx.doi.org/10.1021/ja4035335 | J. Am. Chem. Soc. 2013, 135, 9099–9110

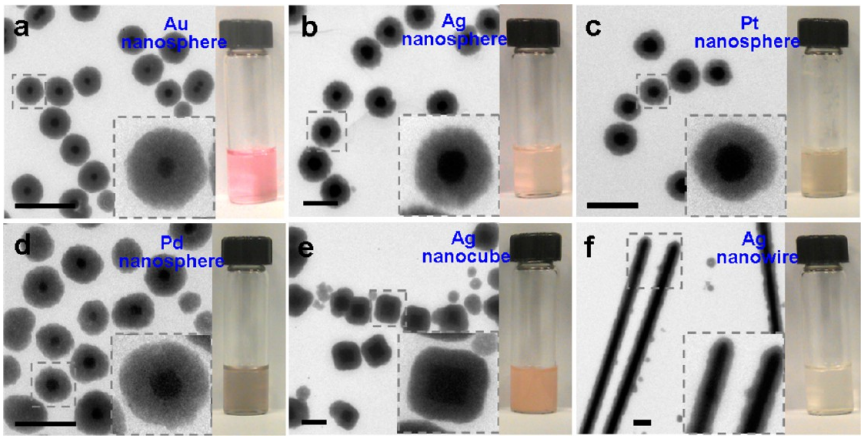

Figure 9. TEM images and photographs of metal@ZnO NPs that were synthesized from different noble metal cores: citrate-stabilized NPs, including (a) Au nanospheres (d_{Au} = 15 nm); (b) Ag nanospheres (d_{Ag} = 60 nm); and (c) Pt nanospheres (d_{Pt} = 40 nm); and PVP-stabilized NPs, including (d) Pd nanospheres (d_{Pd} = 20 nm); (e) Ag nanocubes (d_{Ag} = 150 nm); and (f) AgNWs (d_{AgNW} = 120 nm, l_{AgNW} = 3−5 μm). Insets show magnified views of typical NPs. Scale bar: 200 nm.

nucleation and subsequent heterogeneous nucleation on these newly formed pure ZnO NPs. In the presence of Au seeds, ZnO nucleation can occur at a lower threshold. Once ZnO reaches the critical concentration for path β (C_β), a small ZnO domain will form on the Au seeds. Subsequent ZnO deposition would preferentially occur on the existing ZnO domain (path α), rather than nucleate on a new location of the Au surface (path β, which is more costly). Typically, after the initial nucleation event, the reaction slows due to lower reactant concentrations. Thus, the ZnO oversaturation could be insufficient to support the higher energy β path. This analysis explains the formation of only 1−2 ZnO "petals" on each seed NP (Figures 3c and 6c).

The seed concentration is also an important factor, because the higher is the concentration of seeds in the vicinity, the faster is the ZnO depletion rate. If the seed concentration is too low, ZnO could build up in localized portions of solution that have no seeds, leading to homogeneous nucleation. The resulting pure ZnO NPs will then compete with the ZnO growth on the seeds (see section 10). This lower limit of seed concentration depends on the rates of ZnO formation and diffusion. On the other hand, because the collision probability of NPs is second-order dependent on seed concentration, it cannot be too high to minimize seed aggregation. This upper limit depends on the colloidal stability of the NPs (thermodynamics and/or the rate of effective collision). As a further complication, when the seed NPs aggregate into clusters, their concentration is greatly reduced, diminishing the available nucleation centers for ZnO deposition and causing inefficient ZnO depletion.

When ligand and surfactant were used, the Au−**1**−ZnO or Au−**4**−PVP−ZnO interaction dramatically improved the Au−ZnO interfacial energy. If σ_{13} became close in value to σ_{33}, then the probability of heterogeneous nucleation on Au would be increased. If σ_{13} is small enough, local buildup of ZnO may be sufficient to allow the slightly higher energy β path. In particular, in a region away from the existing ZnO domains, the ZnO buildup can be caused by inefficient diffusion, which should depend on the distance of the nearby ZnO domains and thus the size of the Au seeds. Hence, a small σ_{13} would promote full oxide encapsulation of the seeds both thermodynamically (section 4) and kinetically.

The rate of chemical reactions also played an important role. It is possible that a fast reaction may build up enough material (large ZnO oversaturation) to continually sustain the high energy paths, such as the homogeneous nucleation and the β path. In fact, simultaneously achieving homogeneous and heterogeneous nucleation is known to lead to a large size polydispersity of the resulting NPs.[7] Typically, slow reactions are preferred in the literature to achieve better synthetic control. A fast reaction may promote a large number of nucleation sites per seed, but if it is too fast, it may also cause homogeneous nucleation, leading to polydispersed NPs. In practice, it would be very challenging to maintain the ZnO oversaturation in the small window between C_{homo} and C_β (Figure 8c). Thus, reducing σ_{13} is a more practical solution for promoting multiple nucleation sites (Figure 8b). This approach was effective for the core−shell seed@oxide NPs in our system. For example, the temporal evolution of the Au@ZnO NPs showed that thin ZnO shells (5 nm) already formed at the initial stage and did not form by growing and merging isolated ZnO petals subsequently.[19]

Thus, the choice of reactants is of importance, particularly for the general syntheses of different oxide shells in the following. If the process appears to give rise to homogeneous nucleation, then the oxide oversaturation must be reduced by choosing less reactive starting materials or lower concentrations.

9. General Method for Coating ZnO on Different Seeds. The issues in employing different seeds for ZnO encapsulation are as follows: (a) the initial addition of $Zn(NO_3)_2$ salt can cause the aggregation of the seed NPs; and (b) because the surface ligand on the as-synthesized seeds is usually incompatible, a replacement ligand is required, which should have a stronger binding affinity, sufficient colloidal stability, and a suitable seed−ligand−ZnO interfacial energy. As known in the literature, ligand exchange of colloidal NPs is nothing but trivial, often leading to serious NP aggregation. The use of PVP can alleviate this problem, because it stabilizes the NPs and allows the use of hydrophobic ligands. Once the seeds are fully covered, either via seed−ligand−ZnO or seed−ligand−PVP−ZnO interactions, the growth of ZnO shells thereafter becomes independent of the embedded seeds.

Citrate-stabilized Au,[32] Ag,[33] and Pt nanospheres[34] can be easily coated with ZnO shells using ligand **1** (Figure 9a−c). Pd nanospheres,[35] Ag nanocubes,[36] and Ag nanowires[37] that were stabilized by PVP in their original syntheses can be directly coated with ZnO without addition of a ligand (Figure 9d−f).

dx.doi.org/10.1021/ja4035335 | J. Am. Chem. Soc. 2013, 135, 9099−9110

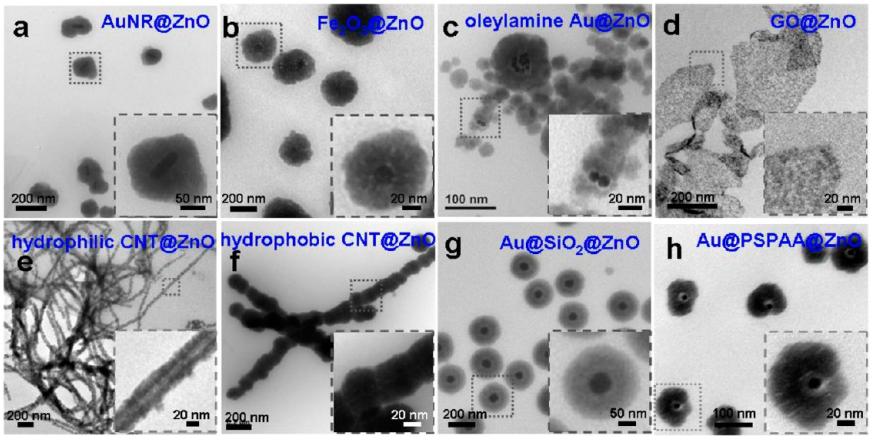

Figure 10. TEM images of the seed@ZnO NPs that were synthesized from different seeds: (a) CTAB-stabilized Au nanorods (d = 20 nm, l = 70−90 nm); (b) oleylamine-stabilized γ-Fe_2O_3 NPs (d = 20 nm); (c) oleylamine-stabilized Au nanospheres (d = 10 nm); (d) GO sheets; (e) bundles of hydrophilic CNTs (d = 15 nm); (f) bundles of hydrophobic CNTs (d = 3 nm); (g) Au@SiO_2 core−shell NPs (d_{Au} = 40 nm); and (h) Au@PSPAA core−shell NPs (d_{Au} = 15 nm). Insets show magnified views of typical NPs.

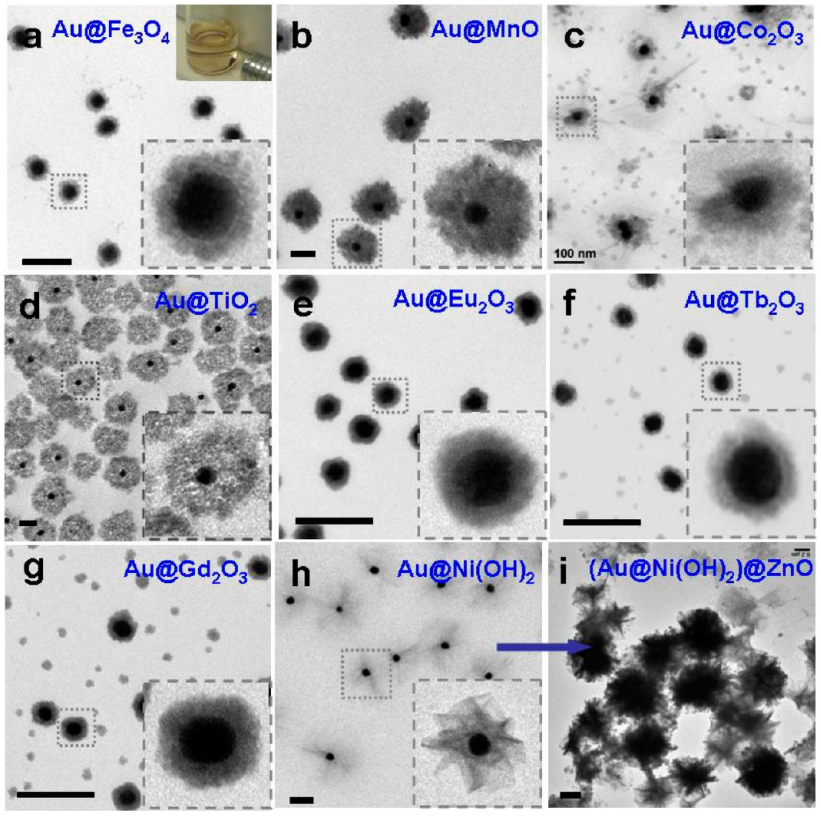

Figure 11. TEM images of the Au@oxide NPs (d_{Au} = 40 nm) with different kinds of oxide shells: (a) Au@Fe_3O_4, (b) Au@MnO, (c) Au@Co_2O_3, (d) Au@TiO_2, (e) Au@Eu_2O_3, (f) Au@Tb_2O_3, (g) Au@Gd_2O_3, (h) Au@$Ni(OH)_2$, and (i) (Au@$Ni(OH)_2$)@ZnO. Insets show magnified views of typical NPs. Scale bar: 200 nm.

The aggregation of these NPs is usually not a problem. For the Ag nanocubes and nanowires, it can be observed that the uniform ZnO shells conformed to the shape of the seeds.

However, for CTAB-stabilized Au nanorods,[38] direct ZnO growth led to pure ZnO NPs and not shells on the nanorods. It is well-known that CTAB binds strongly to Au surface, and it appeared that PVP cannot modify or coat on such CTAB-covered nanorods. Thus, we must use a stronger ligand, such as ligand **1**, to replace CTAB. However, the residual ligand **1** caused ZnO−ZnO aggregation and centrifugation to remove the residual ligand caused Au−Au aggregation. By using a small amount of ligand **1**, full encapsulation of the nanorods could be achieved (as opposed to partial encapsulation), but ZnO−ZnO aggregation remained. The as-synthesized Au nanorods were first centrifuged to remove most of the CTAB, and the concentrated nanorods were dispersed in aqueous PVP with the addition of ligand **1**. After incubation at 60 °C for 2 h, HMTA and $Zn(NO_3)_2$ were added to initiate ZnO formation. As shown in Figure 10a and the Supporting Information, most of the Au nanorods were fully encapsulated.

dx.doi.org/10.1021/ja4035335 | J. Am. Chem. Soc. 2013, 135, 9099−9110

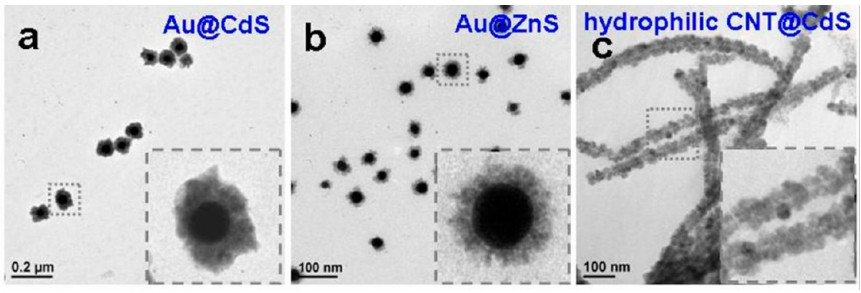

Figure 12. TEM images of (a) Au@CdS (d_{Au} = 40 nm), (b) Au@ZnS (d_{Au} = 30 nm), and (c) bundles of hydrophilic CNTs coated with CdS (CNT@CdS). Insets show magnified views of typical NPs.

For oleylamine-stabilized NPs, the γ-Fe_2O_3 NPs[39] can be easily encapsulated in ZnO but not the corresponding Au NPs,[40] probably because of the weaker oleylamine−Fe_2O_3 interaction and/or the better Fe_2O_3−ZnO interface. The as-purchased Fe_2O_3 NPs were dispersed in THF and then centrifuged to remove most of the oleylamine. These purified Fe_2O_3 NPs were dispersed in PVP solution and used for ZnO coating (Figure 10b). In comparison, the as-synthesized oleylamine-stabilized Au NPs were similarly purified and dispersed in PVP solution. However, ZnO growth at this same stage caused incomplete shells. Thus, ligand **1** was added, which caused aggregation (Figure 10c).

Carbon-based nanomaterials can also be used. Graphene oxide (GO) sheets[41] and oxidized single-wall carbon nanotubes (CNTs)[42] are known to have hydrophilic functional groups (e.g., −OH, −O−, −OOH) on their surface. They were dispersed in aqueous PVP solution, followed by ZnO growth. As shown in Figure 10d,e, a thin layer of ZnO was grown on their surface. Because of the amphiphilic PVP, hydrophobic CNTs can also be coated using the same method (Figure 10f).

An alternative approach is to coat ZnO on top of existing core−shell NPs. Silica and polymer have been widely used for coating NPs. Coating an additional layer of ZnO on an existing shell can test the generality of our method. It is also a method for creating multilayered, hybrid nanostructures. We first prepared Au@silica using ligand **1** to modify the Au surface. After purification, the core−shell NPs can be directly used for ZnO encapsulation in the presence of PVP. While silica does not interact strongly with PVP, the small ZnO−silica interfacial energy allows the full encapsulation of the silica surface by ZnO. This is evident in the TEM image (Figure 10g) where the silica layer has a lighter contrast than the ZnO layer because of the lower electron density of Si than Zn.

We have previously demonstrated that a variety of different NPs can be encapsulated in shells of polystyrene-*block*-poly(acrylic acid) (PSPAA).[43] The resulting polymer shell can serve as an impermeable barrier, isolating the embedded NPs from the environment. The as-synthesized Au@PSPAA core−shell NPs can be purified to remove any interfering agent, and their surface is covered with −COOH groups. Thus, ZnO growth in the presence of PVP can give an additional layer of ZnO on the Au@PSPAA NPs (Figure 10h).

In summary, a wide variety of NPs have been successfully coated with ZnO shells. The method is facile and independent of the composition, size, and geometry of the seeds. However, the problem of exchanging the strong ligands on NP surface was only partially resolved: complete ZnO shells can form, but in a few cases the resulting NPs were aggregated.

10. General Method for Coating Oxides and Sulfides. Using citrate-stabilized Au NPs as model seeds, we explored the coating of oxides and sulfides in general, which mostly appeared to interact strongly with PVP, just like in the case of ZnO. The Au NPs were first modified with ligand **1** and dispersed in aqueous PVP solution. Literature methods were modified in such a way that the reactions of oxide formation were carried out in this seed solution.[19] As shown in Figure 11, various types of oxide shells have been synthesized, including Fe_3O_4,[13] MnO,[44] Co_2O_3,[45] TiO_2,[14a] Eu_2O_3,[46] Tb_2O_3,[47] Gd_2O_3,[48] and β-$Ni(OH)_2$.[49]

A common problem in generating these oxide shells was that their rates of reactions can be quite different. If a large amount of pure oxide NPs was obtained in the product, the reaction needed to be slowed to reduce homogeneous oxide nucleation. Typically, the most effective measure is to use less reactive reactants, but one can also change the solvent, lower the reactant concentration, or increase the seed concentration. In our experiments, the number and size of pure oxide NPs have been greatly reduced. Any remaining small amounts of oxide NPs could be easily removed by centrifugation.

For example, both $FeCl_2$ and $FeCl_3$ can be used to generate iron oxides, but the latter leads to fast reaction, causing the homogeneous nucleation of pure α-Fe_2O_3 spindles.[19] In comparison, $FeCl_2$ reacted slower, allowing the formation of uniform oxides shells, which can be suitably oxidized to give Fe_3O_4. The resulting Au@Fe_3O_4 NPs showed response to an external magnetic field (inset of Figure 11a). Similarly, $MnCl_2$ leads to fast hydrolysis,[19] and thus $Mn(CH_3COO)_2$ was used as the Mn source for generating MnO shells (Figure 11b). In preparing TiO_2 shells, TiF_4 hydrolyzes rapidly, but it is difficult to find a substitute. Thus, we followed the literature method of using ethanol as the solvent,[14a] which reduced the hydrolysis rate and led to successful TiO_2 encapsulation (Figure 11d).

Hydrolysis of $NiCl_2$ in the presence of Au seeds produced shells that appeared more like soft lamellae than solid shells (Figure 11h). XRD measurement showed that the shell is composed of hexagonal structured β-$Ni(OH)_2$.[19] In the literature, β-$Ni(OH)_2$ usually appeared as flakes or platelets,[50] which can be easily converted to NiO by heating.[51] In the presence of PVP, thinner lamellae have also been reported.[52] In our case, the thin lamellae around the seed NPs appeared to be particularly crumbled. To investigate if the crumbling was a result of drying, we coated ZnO on top of the $Ni(OH)_2$ layer. The resulting triple-layer NPs (Figure 11i) still appeared "crumbled", reflecting the existing morphology of the particles in the solution before the ZnO coating.

Using similar methods, metal sulfide shells could be readily prepared using $Na_2S_2O_3$[12] instead of HMTA, under otherwise

dx.doi.org/10.1021/ja4035335 | J. Am. Chem. Soc. 2013, 135, 9099−9110

the same conditions. As examples, we prepared Au@CdS, Au@ZnS core−shell NPs using citrate-stabilized Au seeds (Figure 12a,b). In addition, CNT@CdS core−shell hybrid nanostructures were also prepared, giving an average shell thickness of 20 nm (Figure 12c).

CONCLUSION

In this study, we explored a general synthetic methodology for coating oxide shells on a variety of different seed NPs. The ligand/surfactant of the seed NPs played a critical role in (a) stabilizing the NPs; (b) modulating the oxide-seed interfacial energy; and (c) interfering with the growth of oxide nanocrystals. As summarized in Figure 1, the presence of a good ligand on the seed NPs stabilizes them against salt-induced aggregation, whereas PVP prevents oxide aggregation after the shell formation. While the surfactant PVP is popular in many syntheses, by itself it is usually insufficient to lower the oxide−metal interfacial energy. Thus, an additional ligand is necessary to address the "wetting" issue, via either seed−ligand−oxide or seed−ligand−PVP−oxide interactions. A good ligand is one that can interact strongly with both the core and the shell materials. Formation of pure oxide NPs indicates that the oxide formation is too fast; it can be reduced by slowing the reaction rate or increasing the seed concentration (i.e., faster oxide depletion). Last, while many molecules can interfere with the growth of oxide nanocrystals (e.g., ligands **1** and **4**), they also promote oxide aggregation. PVP remains the optimum choice for a balanced solution for these two problems.

With these understandings, we have achieved an oxide encapsulation method that is rational, general, facile, and scalable. The basic principles can be applied to help rational synthesis of other similar core−shell nanostructures.

EXPERIMENTAL SECTION

Materials. Hexamethylenetetramine (HMTA, Alfa Aesar), $Zn(NO_3)_2{\cdot}6H_2O$ (Sigma), $FeCl_2{\cdot}4H_2O$ (Alfa Aesar), $NiCl_2{\cdot}6H_2O$ (Alfa Aesar), $Mn(CH_3COO)_2{\cdot}4H_2O$ (Sigma-Aldrich), $CoCl_2$ (Alfa Aesar), TiF_4 (Alfa Aesar), $Eu(NO_3)_3{\cdot}5H_2O$ (Sigma), $Tb(NO_3)_3{\cdot}6H_2O$ (Sigma), $GdCl_3{\cdot}6H_2O$ (Alfa Aesar), 4-mercaptobenzoic acid (ligand **1**, Sigma), 2-mercaptoacetic acid (ligand **2**, Alfa Aesar), 11-mercaptoundeconoic acid (ligand **3**, Aldrich), 2-naphthalenethiol (ligand **4**, Sigma), 4-ethylthiolphenol (ligand **5**, Alfa Aesar), 1-octadecanethiol (ligand **6**, Alfa Aesar), 1,2-dipalmitoyl-*sn*-glycero-3-phosphothioethanol (ligand **7**, Avanti), polyvinylpyrrolidone (PVP, M_w = 360 000, 40 000 g mol^{-1}, Sigma-Aldrich), *N*-vinyl-2-pyrrolidone (VP, Sigma-Aldrich), poly(ethylene glycol) (PEG, M_w = 35 000 g mol^{-1}, Alfa Aesar), poly(sodium 4-styrenesulfonate) (PSS, M_w = 90 000 g mol^{-1}, Sigma-Aldrich), Au nanorods (NanoSeedz), γ-Fe_2O_3 NPs (Ocean NanoTech), natural graphite powder (Sigma, 45 μm), and high-quality single-wall carbon nanotubes (with length from 300 nm to 4 μm, carbonaceous purity 99%, NanoIntegris) were used as received. Copper specimen grids (200 mesh) with Formvar/carbon support film (referred to as TEM grids in the text) were purchased from Beijing XXBR Technology Co. All solutions were prepared using ultrapure water (resistance >18 MΩ cm^{-1}).

Au nanospheres (d = 15 and 40 nm),[32] Ag nanospheres (d = 60 nm),[33] Pt nanospheres (d = 40 nm),[34] Pd nanospheres (d = 20 nm),[35] Ag nanowires (d = 120 nm, l = 3−5 μm),[37] Ag nanocubes (d = 150 nm),[36] oleylamine-stabilized Au nanospheres (d = 10 nm),[40] Au@SiO_2 core−shell NPs,[11c] Au@PSPAA core−shell NPs,[43a] graphene oxide (GO),[41] and hydrophilic single wall CNTs[42] were prepared following the literature procedures.

Characterization. Transmission electron microscopy (TEM) images were collected on a JEM-1400 (JEOL) operated at 100−120 kV. High-resolution TEM images were recorded using a Philips CM 300 FEGTEM operating at an accelerating voltage of 300 kV. Fourier transform infrared (FT-IR) spectra were collected on a FT-IR spectrometer (Perkin-Elmer System 2000) using KBr pellets (32 scans), and the spectra were recorded with a resolution of 4 cm^{-1}. Raman spectra were collected from the sample solutions in a cuvette (path length = 1.00 cm) on a PeakSeeker Pro spectrometer (Raman Systems Inc.) using a red laser (λ = 785 nm) at 290 mW. Thermogravimetric analysis (TGA) was conducted with a TA Instruments Q500, and the heating rate was set at 10 °C min^{-1}. X-ray diffraction was performed on a Shimadzu X-ray diffractometer (D/max rA, using Cu K_α radiation at a wavelength of 1.542 Å), and the data were collected from 20° to 80°.

Synthesis of Au@ZnO Core−Shell NPs. Typically, 5 μL of ligand **1** solution (3 mM in ethanol) was added to 1 mL of as-synthesized citrate-stabilized Au NP solution (d = 40 nm) under vortexing, and the mixture was incubated at 60 °C for 2 h. Ligand **1** can be replaced by other ligands **2**−**7**.

For Au NPs modified with hydrophilic ligands (**1**, **2**, or **3**), the solution (an aliquot of 0.5 mL) was concentrated to a total of 10 μL by centrifugation at 6000 rpm (2900g) for 8 min. After the supernatant was removed, the isolated NPs were dispersed in an aqueous PVP solution. For Au NPs modified with hydrophobic ligand (**4**, **5**, **6**, or **7**), the NP solution was not purified; PVP was directly added to this solution to a desired concentration. The mixture solution of PVP and seed NPs was vortexed for 5 s, followed by the addition of HMTA (50 mM, 50 μL). Finally, $Zn(NO_3)_2$ (50 mM, 50 μL) was added. The total volume of the final mixture was 2.5 mL, where [HMTA] = 1 mM, [$Zn(NO_3)_2$] = 1 mM, and [PVP] = 110 mM. After vortexing for 10 s, the reaction mixture was incubated at 95 °C for 3 h.

To isolate the Au@ZnO core−shell NPs, the reaction mixture was centrifuged at 6000 rpm (2900g) for 8 min, the supernatant was removed, and the concentrated NPs were collected at the bottom of the Eppendorf tubes.

General Synthesis of Seed@ZnO Core−Shell NPs. Citrate-stabilized Au nanospheres (d_{Au} = 15 nm), Ag nanospheres (d_{Ag} = 60 nm), and Pt nanospheres (d_{Pt} = 40 nm) were directly treated with ligand **1**. After purification, they were dispersed in aqueous PVP solution, and the above ZnO encapsulation method was applied.

For PVP-stabilized Ag nanocubes, Ag nanowires, and Pd nanospheres, the as-synthesized samples were washed with ethanol for three cycles using centrifugation, to remove the excess PVP and other reactants. The purified NPs were dispersed in PVP solution and used for ZnO encapsulation.

The CTAB-stabilized Au nanorods (50 μL) were first centrifuged to remove most of the CTAB, and the concentrated AuNRs were dispersed in aqueous PVP solution with the addition of ligand **1** (2 mM, 2 μL). This solution was not purified to avoid the aggregation of nanorods. After incubation at 60 °C for 2 h, HMTA and $Zn(NO_3)_2$ were directly added to this solution to initiate ZnO formation.

The oleylamine-stabilized γ-Fe_2O_3 NPs were dispersed in THF and then centrifuged to remove most of the oleylamine. The purified Fe_2O_3 NPs were dispersed in aqueous PVP solution. After that, HMTA (50 mM, 50 μL) and $Zn(NO_3)_2$ (50 mM, 50 μL) were added to this solution to initiate ZnO formation. For oleylamine-stabilized Au NPs in cyclohexane, they were concentrated by centrifugation and then redispersed in 1 mL of THF with the addition of ligand **1** (2 mM, 2 μL). The mixture was incubated at 60 °C for 2 h. Because the ZnO formation was incompatible with THF, the modified AuNPs were isolated by centrifugation (this step caused aggregation) and redispersed in aqueous PVP. Next, HMTA and $Zn(NO_3)_2$ were added to this solution to initiate ZnO formation.

Au@SiO_2 and Au@PSPAA core−shell NPs were purified after the synthesis and directly used as the seeds for ZnO coating in the presence of PVP (ligand was not required).

Aqueous solutions of GO and hydrophilic CNTs were dispersed in aqueous PVP solution and then used for ZnO encapsulation. No additional ligand was necessary. Powder form of hydrophobic CNT was dispersed in aqueous PVP solution using sonication. HMTA and $Zn(NO_3)_2$ then were added to this solution to initiate ZnO formation.

General Synthesis of Au@Oxide Core−Shell NPs. For preparing shells of Fe_3O_4, MnO, Co_2O_3, Eu_2O_3, Tb_2O_3, Gd_2O_3, and

dx.doi.org/10.1021/ja4035335 | J. Am. Chem. Soc. 2013, 135, 9099−9110

β-$Ni(OH)_2$, different metal salts ($FeCl_2$, $Mn(CH_3COO)_2$, $CoCl_2$, $Eu(NO_3)_3$, $Tb(NO_3)_3$, $GdCl_3$, and $NiCl_2$) were used in the place of $Zn(NO_3)_2$, under otherwise identical conditions. The same process was followed, except that lower concentrations were used: [HMTA] = 0.5 mM, [metal salt] = 0.5 mM, and [PVP] = 110 mM.

TiO_2 shell was prepared using a different method. First, 0.04 M of TiF_4 solution was prepared by dissolving TiF_4 powder in a dilute HCl solution with pH value of 2.0, and the mixture was incubated for 1 h. Purified AuNPs (after modification with ligand **1**) then were dispersed in a mixture consisting 1.38 mL of ethanol, 0.07 mL of water, and 0.13 mL of an aqueous PVP solution (200 mM), followed by 0.1 mL of the above TiF_4 (0.04 M) solution. After being sonicated for 10 s, the reaction mixture was incubated at 65 °C for 3 h.

Synthesis of Metal Sulfide Shells. For growing metal sulfide shells, $Na_2S_2O_3$ (0.5 mM) was used in the place of HMTA, while all other conditions were the same.

■ ASSOCIATED CONTENT

Supporting Information

Large-area TEM images and support data for nonessential control experiments. This material is available free of charge via the Internet at http://pubs.acs.org.

■ AUTHOR INFORMATION

Corresponding Author

hongyuchen@ntu.edu.sg; danwang@mail.ipe.ac.cn

Notes

The authors declare no competing financial interest.

■ ACKNOWLEDGMENTS

We thank the A*Star (SERC 112-120-2011) and NRF (CRP-4-2008-06) of Singapore for financial support.

■ REFERENCES

(1) (a) Linic, S.; Christopher, P.; Ingram, D. B. *Nat. Mater.* **2011**, *10*, 911. (b) Liu, Z. W.; Hou, W. B.; Pavaskar, P.; Aykol, M.; Cronin, S. B. *Nano Lett.* **2011**, *11*, 1111. (c) Li, P.; Wei, Z.; Wu, T.; Peng, Q.; Li, Y. *J. Am. Chem. Soc.* **2011**, *133*, 5660.

(2) (a) Atwater, H. A.; Polman, A. *Nat. Mater.* **2010**, *9*, 205. (b) Bayindir, M.; Sorin, F.; Abouraddy, A. F.; Viens, J.; Hart, S. D.; Joannopoulos, J. D.; Fink, Y. *Nature* **2004**, *431*, 826. (c) Abouraddy, A. F.; Bayindir, M.; Benoit, G.; Hart, S. D.; Kuriki, K.; Orf, N.; Shapira, O.; Sorin, F.; Temelkuran, B.; Fink, Y. *Nat. Mater.* **2007**, *6*, 336.

(3) (a) Noginov, M. A.; Zhu, G.; Belgrave, A. M.; Bakker, R.; Shalaev, V. M.; Narimanov, E. E.; Stout, S.; Herz, E.; Suteewong, T.; Wiesner, U. *Nature* **2009**, *460*, 1110. (b) Katzenellenbogen, N.; Grischkowsky, D. *Appl. Phys. Lett.* **1991**, *58*, 222.

(4) (a) Bauer, E. *Z. Kristallogr.* **1958**, *110*, 372. (b) Herman, M. A.; Richter, W.; Sitter, H. *Epitaxy: Physical Principles and Technical Implementation*; Springer: New York, 2004. (c) Peng, Z.; Yang, H. *Nano Today* **2009**, *4*, 143. (d) Habas, S. E.; Lee, H.; Radmilovic, V.; Somorjai, G. A.; Yang, P. *Nat. Mater.* **2007**, *6*, 692. (e) Yang, J.; Peng, J.; Zhang, Q.; Peng, F.; Wang, H.; Yu, H. *Angew. Chem., Int. Ed.* **2009**, *48*, 3991. (f) Huang, S.; Huang, J.; Yang, J.; Peng, J.-J.; Zhang, Q.; Peng, F.; Wang, H.; Yu, H. *Chem.-Eur. J.* **2010**, *16*, 5920. (g) Li, J.; Zeng, H. C. *Angew. Chem., Int. Ed.* **2005**, *44*, 4342. (h) Wang, D. P.; Zeng, H. C. *Chem. Mater.* **2009**, *21*, 4811. (i) Yec, C. C.; Zeng, H. C. *Chem. Mater.* **2012**, *24*, 1917.

(5) Fan, F. R.; Liu, D. Y.; Wu, Y. F.; Duan, S.; Xie, Z. X.; Jiang, Z. Y.; Tian, Z. Q. *J. Am. Chem. Soc.* **2008**, *130*, 6949.

(6) Chen, O.; Zhao, J.; Chauhan, V. P.; Cui, J.; Wong, C.; Harris, D. K.; Wei, H.; Han, H.-S.; Fukumura, D.; Jain, R. K.; Bawendi, M. G. *Nat. Mater.* **2013**, *12*, 445.

(7) Li, W.; Yang, J. P.; Wu, Z. X.; Wang, J. X.; Li, B.; Feng, S. S.; Deng, Y. H.; Zhang, F.; Zhao, D. Y. *J. Am. Chem. Soc.* **2012**, *134*, 11864.

(8) Feng, Y. H.; He, J. T.; Wang, H.; Tay, Y. Y.; Sun, H.; Zhu, L. F.; Chen, H. Y. *J. Am. Chem. Soc.* **2012**, *134*, 2004.

(9) (a) Shi, W. L.; Zeng, H.; Sahoo, Y.; Ohulchanskyy, T. Y.; Ding, Y.; Wang, Z. L.; Swihart, M.; Prasad, P. N. *Nano Lett.* **2006**, *6*, 875. (b) Yu, H.; Chen, M.; Rice, P. M.; Wang, S. X.; White, R. L.; Sun, S. H. *Nano Lett.* **2005**, *5*, 379. (c) Kim, B. Y.; Shim, I. B.; Araci, Z. O.; Saavedra, S. S.; Monti, O. L. A.; Armstrong, N. R.; Sahoo, R.; Srivastava, D. N.; Pyun, J. *J. Am. Chem. Soc.* **2010**, *132*, 3234. (d) Schladt, T. D.; Shukoor, M. I.; Schneider, K.; Tahir, M. N.; Natalio, F.; Ament, I.; Becker, J.; Jochum, F. D.; Weber, S.; Kohler, O.; Theato, P.; Schreiber, L. M.; Sonnichsen, C.; Schroder, H. C.; Muller, W. E. G.; Tremel, W. *Angew. Chem., Int. Ed.* **2010**, *49*, 3976.

(10) Zhang, J.; Tang, Y.; Lee, K.; Ouyang, M. *Science* **2010**, *327*, 1634.

(11) (a) Guerrero-Martinez, A.; Perez-Juste, J.; Liz-Marzan, L. M. *Adv. Mater.* **2010**, *22*, 1182. (b) Seh, Z. W.; Liu, S. H.; Low, M.; Zhang, S. Y.; Liu, Z. L.; Mlayah, A.; Han, M. Y. *Adv. Mater.* **2012**, *24*, 2310. (c) Wong, Y. J.; Zhu, L. F.; Teo, W. S.; Tan, Y. W.; Yang, Y. H.; Wang, C.; Chen, H. Y. *J. Am. Chem. Soc.* **2011**, *133*, 11422.

(12) Sun, Z. H.; Yang, Z.; Zhou, J. H.; Yeung, M. H.; Ni, W. H.; Wu, H. K.; Wang, J. F. *Angew. Chem., Int. Ed.* **2009**, *48*, 2881.

(13) Zhai, Y. M.; Han, L.; Wang, P.; Li, G. P.; Ren, W.; Liu, L.; Wang, E. K.; Dong, S. J. *ACS Nano* **2011**, *5*, 8562.

(14) (a) Lou, X. W.; Archer, L. A. *Adv. Mater.* **2008**, *20*, 1853. (b) Graf, C.; Vossen, D. L. J.; Imhof, A.; van Blaaderen, A. *Langmuir* **2003**, *19*, 6693. (c) Zhang, L.; Blom, D. A.; Wang, H. *Chem. Mater.* **2011**, *23*, 4587.

(15) Fan, F. R.; Ding, Y.; Liu, D. Y.; Tian, Z. Q.; Wang, Z. L. *J. Am. Chem. Soc.* **2009**, *131*, 12036.

(16) (a) Wang, Z. L. *Nano Today* **2010**, *5*, 540. (b) Wang, Z. L. *Annu. Rev. Phys. Chem.* **2004**, *55*, 159. (c) Huang, M. H.; Mao, S.; Feick, H.; Yan, H. Q.; Wu, Y. Y.; Kind, H.; Weber, E.; Russo, R.; Yang, P. D. *Science* **2001**, *292*, 1897.

(17) Zhu, L. F.; Wang, H.; Shen, X. S.; Chen, L. Y.; Wang, Y. W.; Chen, H. Y. *Small* **2012**, *8*, 1857.

(18) (a) Yan, Z. J.; Ma, Y. W.; Wang, D. L.; Wang, J. H.; Gao, Z. S.; Song, T. *J. Phys. Chem. C* **2008**, *112*, 9219. (b) Yao, K. X.; Zeng, H. C. *J. Phys. Chem. C* **2007**, *111*, 13301.

(19) See the Supporting Information for details.

(20) Xu, S.; Wang, Z. L. *Nano Res.* **2011**, *4*, 1013.

(21) Zhou, T. J.; Lu, M. H.; Zhang, Z. H.; Gong, H.; Chin, W. S.; Liu, B. *Adv. Mater.* **2010**, *22*, 403.

(22) Liu, Z.; Wen, X. D.; Wu, X. L.; Gao, Y. J.; Chen, H. T.; Zhu, J.; Chu, P. K. *J. Am. Chem. Soc.* **2009**, *131*, 9405.

(23) Wang, L. Y.; Luo, J.; Maye, M. M.; Fan, Q.; Qiang, R. D.; Engelhard, M. H.; Wang, C. M.; Lin, Y. H.; Zhong, C. J. *J. Mater. Chem.* **2005**, *15*, 1821.

(24) (a) Tian, Z.-Q.; Ren, B.; Wu, D.-Y. *J. Phys. Chem. B* **2002**, *106*, 9463. (b) Campion, A.; Kambhampati, P. *Chem. Soc. Rev.* **1998**, *27*, 241.

(25) Feng, Y. H.; Wang, Y.; Wang, H.; Chen, T.; Tay, Y. Y.; Yao, L.; Yan, Q. Y.; Li, S. Z.; Chen, H. Y. *Small* **2012**, *8*, 246.

(26) Feng, Y. H.; Xing, S. X.; Xu, J.; Wang, H.; Lim, J. W.; Chen, H. Y. *Dalton Trans.* **2010**, *39*, 349.

(27) Torza, S.; Mason, S. G. *J. Colloid Interface Sci.* **1970**, *33*, 67.

(28) Lu, G.; Li, S. Z.; Guo, Z.; Farha, O. K.; Hauser, B. G.; Qi, X. Y.; Wang, Y.; Wang, X.; Han, S. Y.; Liu, X. G.; DuChene, J. S.; Zhang, H.; Zhang, Q. C.; Chen, X. D.; Ma, J.; Loo, S. C. J.; Wei, W. D.; Yang, Y. H.; Hupp, J. T.; Huo, F. W. *Nat. Chem.* **2012**, *4*, 310.

(29) Music, S.; Saric, A.; Popovic, S. *J. Alloys Compd.* **2008**, *448*, 277.

(30) Song, R. Q.; Colfen, H. *Adv. Mater.* **2010**, *22*, 1301.

(31) Zhang, Q. F.; Chou, T. R.; Russo, B.; Jenekhe, S. A.; Cao, G. Z. *Angew. Chem., Int. Ed.* **2008**, *47*, 2402.

(32) Frens, G. *Nat. Phys. Sci.* **1973**, *241*, 20.

(33) Chen, G.; Wang, Y.; Yang, M. X.; Xu, J.; Goh, S. J.; Pan, M.; Chen, H. Y. *J. Am. Chem. Soc.* **2010**, *132*, 3644.

(34) Bigall, N. C.; Hartling, T.; Klose, M.; Simon, P.; Eng, L. M.; Eychmuller, A. *Nano Lett.* **2008**, *8*, 4588.

(35) Xiong, Y. J.; McLellan, J. M.; Yin, Y. D.; Xia, Y. N. *Angew. Chem., Int. Ed.* **2007**, *46*, 790.
(36) Zhang, Q. A.; Li, W. Y.; Wen, L. P.; Chen, J. Y.; Xia, Y. N. *Chem.-Eur. J.* **2010**, *16*, 10234.
(37) Sun, Y. G.; Xia, Y. N. *Adv. Mater.* **2002**, *14*, 833.
(38) Nikoobakht, B.; El-Sayed, M. A. *Chem. Mater.* **2003**, *15*, 1957.
(39) Xu, Z. C.; Shen, C. M.; Hou, Y. L.; Gao, H. J.; Sun, S. S. *Chem. Mater.* **2009**, *21*, 1778.
(40) Zhang, M.; Cushing, B. L.; O'Connor, C. J. *Nanotechnology* **2008**, 19.
(41) Park, S.; Ruoff, R. S. *Nat. Nanotechnol.* **2009**, *4*, 217.
(42) Chen, L. Y.; Yu, S. Z.; Wang, H.; Xu, J.; Liu, C. C.; Chong, W. H.; Chen, H. Y. *J. Am. Chem. Soc.* **2013**, *135*, 835.
(43) (a) Wang, H.; Chen, L.; Shen, X.; Zhu, L.; He, J.; Chen, H. *Angew. Chem., Int. Ed.* **2012**, *51*, 8021. (b) Xu, J.; Wang, H.; Liu, C.; Yang, Y.; Chen, T.; Wang, Y.; Wang, F.; Liu, X.; Xing, B.; Chen, H. *J. Am. Chem. Soc.* **2010**, *132*, 11920. (c) Liu, C.; Chen, G.; Sun, H.; Xu, J.; Feng, Y.; Zhang, Z.; Wu, T.; Chen, H. *Small* **2011**, *7*, 2721. (d) Chen, G.; Wang, Y.; Yang, M.; Xu, J.; Goh, S. J.; Pan, M.; Chen, H. *J. Am. Chem. Soc.* **2010**, *132*, 3644. (e) Wang, H.; Chen, L.; Feng, Y.; Chen, H. *Acc. Chem. Res.* **2013**, DOI: 10.1021/ar400020j.
(44) An, G. M.; Yu, P.; Xiao, M. J.; Liu, Z. M.; Miao, Z. J.; Ding, K. L.; Mao, L. Q. *Nanotechnology* **2008**, *19*, 275709.
(45) Lin, H. K.; Chiu, H. C.; Tsai, H. C.; Chien, S. H.; Wang, C. B. *Catal. Lett.* **2003**, *88*, 169.
(46) Wu, G. S.; Zhang, L. D.; Cheng, B. C.; Xie, T.; Yuan, X. Y. *J. Am. Chem. Soc.* **2004**, *126*, 5976.
(47) Qu, D. L.; Xie, F. Y.; Meng, H.; Gong, L.; Zhang, W. H.; Chen, J.; Li, G. R.; Liu, P.; Tong, Y. X. *J. Phys. Chem. C* **2010**, *114*, 1424.
(48) Li, I. F.; Su, C. H.; Sheu, H. S.; Chiu, H. C.; Lo, Y. W.; Lin, W. T.; Chen, J. H.; Yeh, C. S. *Adv. Funct. Mater.* **2008**, *18*, 766.
(49) Shao, M. F.; Ning, F. Y.; Zhao, J. W.; Wei, M.; Evans, D. G.; Duan, X. *J. Am. Chem. Soc.* **2012**, *134*, 1071.
(50) Liu, L.; Li, Y.; Yuan, S.; Ge, M.; Ren, M.; Sun, C.; Zhou, Z. *J. Phys. Chem. C* **2010**, *114*, 251.
(51) Ren, Y.; Gao, L. A. *J. Am. Ceram. Soc.* **2010**, *93*, 3560.
(52) Buscaglia, M. T.; Buscaglia, V.; Bottino, C.; Viviani, M.; Fournier, R.; Sennour, M.; Presto, S.; Marazza, R.; Nanni, P. *Cryst. Growth Des.* **2008**, *8*, 3847.